

000 054
 001 055
 002 056
 003 057
 004 058
 005 059
 006 060
 007 061
 008 062
 009 063
 010 064
 011 065
 012 066
 013 067
 014 068
 015 069
 016 070
 017 071
 018 072
 019 073
 020 074
 021 075
 022 076
 023 077
 024 078
 025 079
 026 080
 027 081
 028 082
 029 083
 030 084
 031 085
 032 086
 033 087
 034 088
 035 089
 036 090
 037 091
 038 092
 039 093
 040 094
 041 095
 042 096
 043 097
 044 098
 045 099
 046 100
 047 101
 048 102
 049 103
 050 104
 051 105
 052 106
 053 107

Supplementary Materials to ‘‘Multi-channel Weighted Nuclear Norm Minimization for Real Color Image Denoising’’

Anonymous ICCV submission

Paper ID 572

In this supplementary file, we provide:

1. The proof of the Theorem 1 in the main paper;
2. More denoising results on the Kodak PhotoCD dataset;
3. More visual comparisons of denoised images on the real noisy images of dataset [1];
4. More visual comparisons of denoised images on the real noisy images of dataset [2].

1. Proof of Theorem 1.

Theorem 1. Assume that the weights in w are in a non-descending order, the sequence $\{\mathbf{X}_k\}$, $\{\mathbf{Z}_k\}$, and $\{\mathbf{A}_k\}$ generated in Algorithm 1 satisfy:

$$(a) \lim_{k \rightarrow \infty} \|\mathbf{X}_{k+1} - \mathbf{Z}_{k+1}\|_F = 0; \quad (b) \lim_{k \rightarrow \infty} \|\mathbf{X}_{k+1} - \mathbf{X}_k\|_F = 0; \quad (c) \lim_{k \rightarrow \infty} \|\mathbf{Z}_{k+1} - \mathbf{Z}_k\|_F = 0. \quad (1)$$

Proof. 1. Firstly, we prove that the sequence $\{\mathbf{A}_k\}$ generated by Algorithm 1 is upper bounded. Let $\mathbf{X}_{k+1} + \rho_k^{-1} \mathbf{A}_k = \mathbf{U}_k \Sigma_k \mathbf{V}_k^\top$ be its singular value decomposition (SVD) [3] in the $(k+1)$ -th iteration. According to Corollary 1 of [4], we can have the SVD of \mathbf{Z}_{k+1} as $\mathbf{Z}_{k+1} = \mathbf{U}_k \hat{\Sigma}_k \mathbf{V}_k^\top = \mathbf{U}_k \mathcal{S}_{\frac{w}{\rho_k}}(\Sigma_k) \mathbf{V}_k^\top$. Then we have

$$\|\mathbf{A}_{k+1}\|_F = \|\mathbf{A}_k + \rho_k(\mathbf{X}_{k+1} - \mathbf{Z}_{k+1})\|_F = \rho_k \|\rho_k^{-1} \mathbf{A}_k + \mathbf{X}_{k+1} - \mathbf{Z}_{k+1}\|_F \quad (2)$$

$$= \rho_k \|\mathbf{U}_k \Sigma_k \mathbf{V}_k^\top - \mathbf{U}_k \mathcal{S}_{\frac{w}{\rho_k}}(\Sigma_k) \mathbf{V}_k^\top\|_F = \rho_k \|\Sigma_k - \mathcal{S}_{\frac{w}{\rho_k}}(\Sigma_k)\|_F \quad (3)$$

$$= \rho_k \sqrt{\sum_i (\Sigma_k^{ii} - \mathcal{S}_{\frac{w}{\rho_k}}(\Sigma_k^{ii}))^2} \leq \rho_k \sqrt{\sum_i (\frac{w_i}{\rho_k})^2} = \sqrt{\sum_i w_i^2}. \quad (4)$$

The inequality in the second last step can be proved as follows: given the diagonal matrix Σ_k , we define Σ_k^{ii} as the i -th element of Σ_k^{ii} . If $\Sigma_k^{ii} \geq \frac{w_i}{\rho_k}$, we have $\mathcal{S}_{\frac{w}{\rho_k}}(\Sigma_k^{ii}) = \Sigma_k^{ii} - \frac{w_i}{\rho_k}$. If $\Sigma_k^{ii} < \frac{w_i}{\rho_k}$, we have $\mathcal{S}_{\frac{w}{\rho_k}}(\Sigma_k^{ii}) = 0$. Overall, we have $|\Sigma_k^{ii} - \mathcal{S}_{\frac{w}{\rho_k}}(\Sigma_k^{ii})| \leq \frac{w_i}{\rho_k}$ and hence the inequality holds. Hence, the sequence $\{\mathbf{A}_k\}$ is upper bounded.

2. Secondly, we prove that the sequence of Lagrangian function $\{\mathcal{L}(\mathbf{X}_{k+1}, \mathbf{Z}_{k+1}, \mathbf{A}_k, \rho_k)\}$ is also upper bounded. Since we have the globally optimal solution of \mathbf{X} and \mathbf{Z} in their corresponding subproblems, we always have

$$\mathcal{L}(\mathbf{X}_{k+1}, \mathbf{Z}_{k+1}, \mathbf{A}_k, \rho_k) \leq \mathcal{L}(\mathbf{X}_k, \mathbf{Z}_k, \mathbf{A}_k, \rho_k). \quad (5)$$

Based on the updating rule that $\mathbf{A}_{k+1} = \mathbf{A}_k + \rho_k(\mathbf{X}_{k+1} - \mathbf{Z}_{k+1})$, we have

$$\mathcal{L}(\mathbf{X}_{k+1}, \mathbf{Z}_{k+1}, \mathbf{A}_{k+1}, \rho_{k+1}) \quad (6)$$

$$= \mathcal{L}(\mathbf{X}_{k+1}, \mathbf{Z}_{k+1}, \mathbf{A}_k, \rho_k) + \langle \mathbf{A}_{k+1} - \mathbf{A}_k, \mathbf{X}_{k+1} - \mathbf{Z}_{k+1} \rangle + \frac{\rho_{k+1} - \rho_k}{2} \|\mathbf{X}_{k+1} - \mathbf{Z}_{k+1}\|_F^2 \quad (7)$$

$$= \mathcal{L}(\mathbf{X}_{k+1}, \mathbf{Z}_{k+1}, \mathbf{A}_k, \rho_k) + \frac{\rho_{k+1} + \rho_k}{2\rho_k^2} \|\mathbf{A}_{k+1} - \mathbf{A}_k\|_F^2. \quad (8)$$

108 Since the sequence $\{\mathbf{A}_k\}$ is upper bounded, the sequence $\{\mathbf{A}_{k+1} - \mathbf{A}_k\}$ is also upper bounded. Denote by a the upper bound
 109 of $\{\mathbf{A}_{k+1} - \mathbf{A}_k\}$, i.e., $\|\mathbf{A}_{k+1} - \mathbf{A}_k\|_F \leq a$, we have
 110

$$\begin{aligned} 111 \quad \mathcal{L}(\mathbf{X}_{k+1}, \mathbf{Z}_{k+1}, \mathbf{A}_{k+1}, \rho_{k+1}) &\leq \mathcal{L}(\mathbf{X}_1, \mathbf{Z}_1, \mathbf{A}_0, \rho_0) + a^2 \sum_{k=0}^{\infty} \frac{\rho_{k+1} + \rho_k}{2\rho_k^2} \\ 112 \end{aligned} \quad (9)$$

$$\begin{aligned} 113 \quad &= \mathcal{L}(\mathbf{X}_1, \mathbf{Z}_1, \mathbf{A}_0, \rho_0) + a^2 \sum_{k=0}^{\infty} \frac{\mu + 1}{2\mu^k \rho_0} \\ 114 \end{aligned} \quad (10)$$

$$\begin{aligned} 115 \quad &\leq \mathcal{L}(\mathbf{X}_1, \mathbf{Z}_1, \mathbf{A}_0, \rho_0) + \frac{a^2}{\rho_0} \sum_{k=0}^{\infty} \frac{1}{\mu^{k-1}}. \\ 116 \end{aligned} \quad (11)$$

117 The last inequality holds since $\mu > 1$ and $\mu + 1 < 2\mu$. Therefore, we have $\sum_{k=0}^{\infty} \frac{1}{\mu^{k-1}} < \infty$ and the sequence of Lagrangian
 118 function $\{\mathcal{L}(\mathbf{X}_{k+1}, \mathbf{Z}_{k+1}, \mathbf{A}_{k+1}, \rho_{k+1})\}$ is upper bounded.
 119

120 3. Thirdly, we prove that the sequences of $\{\mathbf{X}_k\}$ and $\{\mathbf{Z}_k\}$ are upper bounded. Since
 121

$$\begin{aligned} 122 \quad \|\mathbf{W}(\mathbf{Y} - \mathbf{X}_k)\|_F^2 + \|\mathbf{Z}_k\|_{\mathbf{w},*} = \mathcal{L}(\mathbf{X}_k, \mathbf{Z}_k, \mathbf{A}_{k-1}, \rho_{k-1}) - \langle \mathbf{A}_k, \mathbf{X}_k - \mathbf{Z}_k \rangle - \frac{\rho_k}{2} \|\mathbf{X}_k - \mathbf{Z}_k\|_F^2 \\ 123 \end{aligned} \quad (12)$$

$$\begin{aligned} 124 \quad &= \mathcal{L}(\mathbf{X}_k, \mathbf{Z}_k, \mathbf{A}_{k-1}, \rho_{k-1}) + \frac{1}{2\rho_k} (\|\mathbf{A}_{k-1}\|_F^2 - \|\mathbf{A}_k\|_F^2), \\ 125 \end{aligned} \quad (13)$$

126 both $\{\mathbf{W}(\mathbf{Y} - \mathbf{X}_k)\}$ and $\{\mathbf{Z}_k\}$ are upper bounded, and hence the sequence $\{\mathbf{X}_k\}$ is bounded by the Cauchy-Schwarz
 127 inequality and triangle inequality. We can obtain that
 128

$$\lim_{k \rightarrow \infty} \|\mathbf{X}_{k+1} - \mathbf{Z}_{k+1}\|_F = \lim_{k \rightarrow \infty} \rho_k^{-1} \|\mathbf{A}_{k+1} - \mathbf{A}_k\|_F = 0, \quad (14)$$

129 and the equation (a) is proved.
 130

131 4. Then we can prove that

$$\begin{aligned} 132 \quad \lim_{k \rightarrow \infty} \|\mathbf{X}_{k+1} - \mathbf{X}_k\|_F &= \lim_{k \rightarrow \infty} \|(\mathbf{W}^\top \mathbf{W} + \frac{\rho_k}{2} \mathbf{I})^{-1} (\mathbf{W}^\top \mathbf{W} \mathbf{Y} - \mathbf{W}^\top \mathbf{W} \mathbf{Z}_k - \frac{1}{2} \mathbf{A}_k) - \rho_k^{-1} (\mathbf{A}_k - \mathbf{A}_{k-1})\|_F \\ 133 \end{aligned} \quad (15)$$

$$\begin{aligned} 134 \quad &\leq \lim_{k \rightarrow \infty} \|(\mathbf{W}^\top \mathbf{W} + \frac{\rho_k}{2} \mathbf{I})^{-1} (\mathbf{W}^\top \mathbf{W} \mathbf{Y} - \mathbf{W}^\top \mathbf{W} \mathbf{Z}_k - \frac{1}{2} \mathbf{A}_k)\|_F + \rho_k^{-1} \|\mathbf{A}_k - \mathbf{A}_{k-1}\|_F \\ 135 \end{aligned} \quad (16)$$

$$= 0, \quad (17)$$

136 and hence the equation (b) is proved.
 137

138 5. Finally, the equation (c) can be proved by checking that

$$\begin{aligned} 139 \quad \lim_{k \rightarrow \infty} \|\mathbf{Z}_{k+1} - \mathbf{Z}_k\|_F &= \lim_{k \rightarrow \infty} \|\mathbf{X}_k + \rho_k^{-1} \mathbf{A}_{k-1} - \mathbf{Z}_k + \mathbf{X}_{k+1} - \mathbf{X}_k + \rho_k^{-1} \mathbf{A}_{k-1} + \rho_k^{-1} \mathbf{A}_k - \rho_k^{-1} \mathbf{A}_{k+1}\|_F \\ 140 \end{aligned} \quad (18)$$

$$\leq \lim_{k \rightarrow \infty} (\|\Sigma_{k-1} - \mathcal{S}_{\mathbf{w}/\rho_{k-1}}(\Sigma_{k-1})\|_F + \|\mathbf{X}_{k+1} - \mathbf{X}_k\|_F + \rho_k^{-1} \|\mathbf{A}_{k-1} + \mathbf{A}_{k+1} - \mathbf{A}_k\|_F) \quad (19)$$

$$\leq \lim_{k \rightarrow \infty} (\rho_{k-1}^{-1} \|\mathbf{w}\|_F + \|\mathbf{X}_{k+1} - \mathbf{X}_k\|_F + \rho_k^{-1} \|\mathbf{A}_{k-1} + \mathbf{A}_{k+1} - \mathbf{A}_k\|_F) \quad (20)$$

$$= 0, \quad (21)$$

141 where $\mathbf{U}_{k-1} \Sigma_{k-1} \mathbf{V}_{k-1}^\top$ is the SVD of the matrix $\mathbf{X}_k + \rho_{k-1} \mathbf{A}_{k-1}$. □
 142

143

144 2. More denoising results on the Kodak PhotoCD dataset

145 In the main paper, we have given the PSNR results of the competing methods on the 24 high quality images from the
 146 Kodak PhotoCD dataset when the standard deviations of the additive white Gaussian noise (AWGN) are $\sigma_r = 40, \sigma_g = 20, \sigma_b = 30$ for R, G, B channels, respectively. Here we provide more denoising results on this dataset. In Tables 1-3,
 147 we give the PSNR results on these images when the noise standard deviations are $\sigma_r = 40, \sigma_g = 20, \sigma_b = 30$ in Table 1,
 148 $\sigma_r = 30, \sigma_g = 10, \sigma_b = 50$ in Table 2 and $\sigma_r = 5, \sigma_g = 30, \sigma_b = 15$ in Table 3, respectively. In Figures 1-6, we give the
 149 visual comparisons of the denoised images by different methods.
 150

151

152

153

154

155

156

157

158

159

160

161

Table 1. PSNR(dB) results of different denoising methods on the Kodak PhotoCD dataset.

Image#	$\sigma_r = 40, \sigma_g = 20, \sigma_b = 30$								
	CBM3D	MLP	TNRD	NI	NC	WNNM-1	WNNM-2	WNNM-3	MC-WNNM
1	25.24	25.70	25.74	23.85	24.90	26.01	25.95	25.58	26.66
2	28.27	30.12	30.21	25.90	25.87	30.08	30.11	29.80	30.20
3	28.81	31.19	31.49	26.00	28.58	31.58	31.61	31.20	32.25
4	27.95	29.88	29.86	25.82	25.67	30.13	30.16	29.84	30.49
5	25.03	26.00	26.18	24.38	25.15	26.44	26.39	25.32	26.82
6	26.24	26.84	26.90	24.65	24.74	27.39	27.30	26.88	27.98
7	27.88	30.28	30.40	25.63	27.69	30.47	30.54	29.70	30.98
8	25.05	25.59	25.83	24.02	25.30	26.71	26.75	25.26	26.90
9	28.44	30.75	30.81	25.94	27.44	30.86	30.92	30.29	31.49
10	28.27	30.38	30.57	25.87	28.42	30.65	30.68	29.95	31.26
11	26.95	28.00	28.14	25.32	24.67	28.19	28.16	27.61	28.63
12	28.76	30.87	31.05	26.01	28.37	30.97	31.06	30.58	31.48
13	23.76	23.95	23.99	23.53	22.76	24.27	24.15	23.52	24.89
14	26.02	26.97	27.11	24.94	25.68	27.20	27.15	26.55	27.57
15	28.38	30.15	30.44	26.06	28.21	30.52	30.60	30.13	30.81
16	27.75	28.82	28.87	25.69	26.66	29.27	29.21	29.02	29.96
17	27.90	29.57	29.80	25.85	28.32	29.78	29.79	29.16	30.40
18	25.77	26.40	26.41	24.74	25.70	26.63	26.56	26.01	27.22
19	27.30	28.67	28.81	25.40	26.52	29.19	29.22	28.67	29.57
20	28.96	30.40	30.76	24.95	25.90	30.79	30.83	29.97	31.07
21	26.54	27.53	27.60	25.06	26.48	27.80	27.75	27.12	28.34
22	27.05	28.17	28.27	25.36	26.60	28.21	28.16	27.81	28.64
23	29.14	32.31	32.51	26.13	23.24	31.89	31.97	31.21	32.34
24	25.75	26.41	26.53	24.55	25.73	27.10	27.03	26.18	27.59
Average	27.13	28.54	28.68	25.24	26.19	28.84	28.83	28.22	29.31

Table 2. PSNR(dB) results of different denoising methods on the Kodak PhotoCD dataset.

Image#	$\sigma_r = 30, \sigma_g = 10, \sigma_b = 50$								
	CBM3D	MLP	TNRD	NI	NC	WNNM-1	WNNM-2	WNNM-3	MC-WNNM
1	23.38	26.49	26.50	24.82	23.59	26.40	25.60	24.76	27.81
2	25.19	30.94	30.90	26.82	27.79	30.89	29.75	29.21	30.96
3	25.39	32.03	32.09	27.52	27.41	32.20	31.17	30.39	32.89
4	24.96	30.55	30.47	27.34	27.00	30.74	29.71	29.10	31.19
5	23.29	26.65	26.73	25.72	26.67	26.74	25.98	24.68	27.60
6	24.09	27.76	27.70	26.10	26.12	27.85	26.96	26.01	29.15
7	24.89	30.70	30.72	27.17	28.07	30.91	29.94	28.87	31.37
8	23.30	26.12	26.27	25.59	26.11	26.87	26.33	24.74	27.44
9	25.20	31.35	31.31	27.74	28.33	31.30	30.45	29.44	32.08
10	25.13	31.01	31.05	27.60	28.53	31.12	30.17	29.21	31.83
11	24.54	28.79	28.82	26.72	24.40	28.73	27.79	26.94	29.60
12	25.43	31.60	31.60	27.82	29.01	31.59	30.62	29.91	32.11
13	22.50	24.71	24.73	24.96	23.36	24.70	23.85	22.86	25.96
14	23.91	27.69	27.72	26.26	23.08	27.62	26.81	25.91	28.57
15	25.45	31.09	31.05	27.36	28.49	31.29	30.21	29.46	31.39
16	24.89	29.79	29.73	27.35	27.10	29.84	28.85	28.13	31.10
17	25.12	30.26	30.24	27.15	27.54	30.11	29.35	28.43	31.08
18	23.83	27.26	27.26	26.05	26.15	27.32	26.18	25.28	28.32
19	24.63	29.40	29.39	27.06	27.41	29.78	28.87	28.05	30.53
20	26.43	31.16	31.27	26.43	26.92	31.25	30.43	29.41	31.55
21	24.24	28.26	28.27	26.66	27.18	28.22	27.45	26.40	29.29
22	24.51	29.03	29.06	26.83	27.64	29.02	27.81	27.18	29.57
23	25.55	32.87	32.75	27.60	23.75	32.58	31.46	30.50	32.34
24	23.85	27.06	27.13	25.86	27.05	27.50	26.63	25.55	28.32
Average	24.57	29.27	29.28	26.69	26.61	29.36	28.43	27.52	30.09

324 Table 3. PSNR(dB) results of different denoising methods on the Kodak PhotoCD dataset. 378
325

Image#	$\sigma_r = 5, \sigma_g = 30, \sigma_b = 15$								
	CBM3D	MLP	TNRD	NI	NC	WNNM-1	WNNM-2	WNNM-3	MC-WNNM
1	27.25	28.06	28.62	25.00	29.55	28.16	27.95	28.15	30.20
2	29.70	31.30	32.70	27.80	29.69	32.54	31.60	31.73	34.04
3	30.34	31.98	34.07	28.02	31.93	33.91	33.68	33.52	35.55
4	29.47	31.10	32.56	27.70	32.56	32.68	31.85	31.90	34.06
5	27.31	28.59	29.35	26.14	30.00	28.83	29.00	28.91	30.05
6	28.20	29.10	29.90	26.15	28.81	29.55	29.46	29.62	31.64
7	29.73	31.60	33.46	27.22	31.63	33.09	33.29	32.86	34.24
8	27.47	28.16	28.91	25.34	30.16	29.15	29.24	29.03	29.91
9	30.07	31.63	33.55	27.86	31.54	33.19	33.20	32.95	34.53
10	29.96	31.37	33.20	27.74	33.44	32.98	33.02	32.74	34.38
11	28.73	29.85	30.87	26.98	30.16	30.45	30.14	30.21	32.10
12	30.20	31.50	33.31	27.97	31.69	33.22	32.71	32.65	34.64
13	26.18	26.69	26.98	25.14	27.97	26.49	26.42	26.62	28.30
14	27.86	29.07	29.87	26.67	29.21	29.36	29.14	29.30	31.18
15	29.91	31.58	33.13	28.04	31.17	33.22	32.34	32.36	34.27
16	29.29	30.35	31.54	27.46	32.18	31.34	31.05	31.21	33.72
17	29.50	31.09	32.52	27.81	32.80	32.09	32.00	31.85	33.61
18	27.72	28.74	29.36	26.57	28.63	28.88	28.76	28.89	30.56
19	28.98	30.18	31.35	27.25	29.79	31.34	30.77	30.95	33.10
20	30.63	31.78	33.27	27.89	29.52	33.00	32.55	32.58	34.18
21	28.50	29.58	30.54	26.86	30.99	30.02	30.03	30.03	31.69
22	28.61	29.78	30.82	27.19	30.50	30.47	29.82	30.10	32.08
23	30.60	32.66	35.06	28.17	32.82	34.72	34.37	33.94	35.16
24	27.97	28.81	29.61	26.01	30.75	29.47	29.35	29.39	30.93
Average	28.92	30.19	31.44	27.04	30.73	31.17	30.91	30.89	32.67

350

3. More visual comparisons of denoised images on the real noisy images of dataset [1]

 404
351

In this section, we give more comparisons of the state-of-the-art denoising methods on dataset [1]. The real noisy images in dataset [1] have no “ground truth” images and hence we only compare the visual quality of the denoised images by different methods. As can be seen from Figures 7-10, the proposed MC-WNNM method performs better than the competing methods.

355

4. More visual comparisons of denoised images on the real noisy images of dataset [2]

 409
356

In this section, we provide more comparisons of the proposed method with the state-of-the-art denoising methods on the 15 cropped real noisy images used in [2]. In this dataset, each scene was shot 500 times under the same camera and camera setting. The mean image of the 500 shots is roughly taken as the “ground truth”, with which the PSNR can be computed. As can be seen from Figures 11-14, our proposed method achieves better performance than the the competing methods. This validates the effectiveness of the proposed MC-WNNM method for real noisy image denoising.

432
433
434
435
436
437
438
439
440
441
442
443
444
445
446
447
448
449
450
451
452
453
454
455
456
457
458
459
460
461
462
463
464
465
466
467
468
469
470
471
472
473
474
475
476
477
478
479
480
481
482
483
484
485

486
487
488
489
490
491
492
493
494
495
496
497
498
499
500
501
502
503
504
505
506
507
508
509
510
511
512
513
514
515
516
517
518
519
520
521
522
523
524
525
526
527
528
529
530
531
532
533
534
535
536
537
538
539



Figure 1. Denoised images of different methods on the image “kodim01” degraded by AWGN with different standard deviations of $\sigma_r = 40$, $\sigma_g = 20$, $\sigma_b = 30$ on R, G, B channels, respectively. The images are better to be zoomed in on screen.

540
541
542
543
544
545
546
547
548594
595
596
597
598
599
600
601
602
603
604
605
606
607
608
609
610
611
612
613549
550
551
552
553
554
555
556
557
558603
604
605
606
607
608
609
610
611
612
613

559

614

560
561
562
563
564
565
566
567
568
569
570615
616
617
618
619
620
621
622
623
624

571

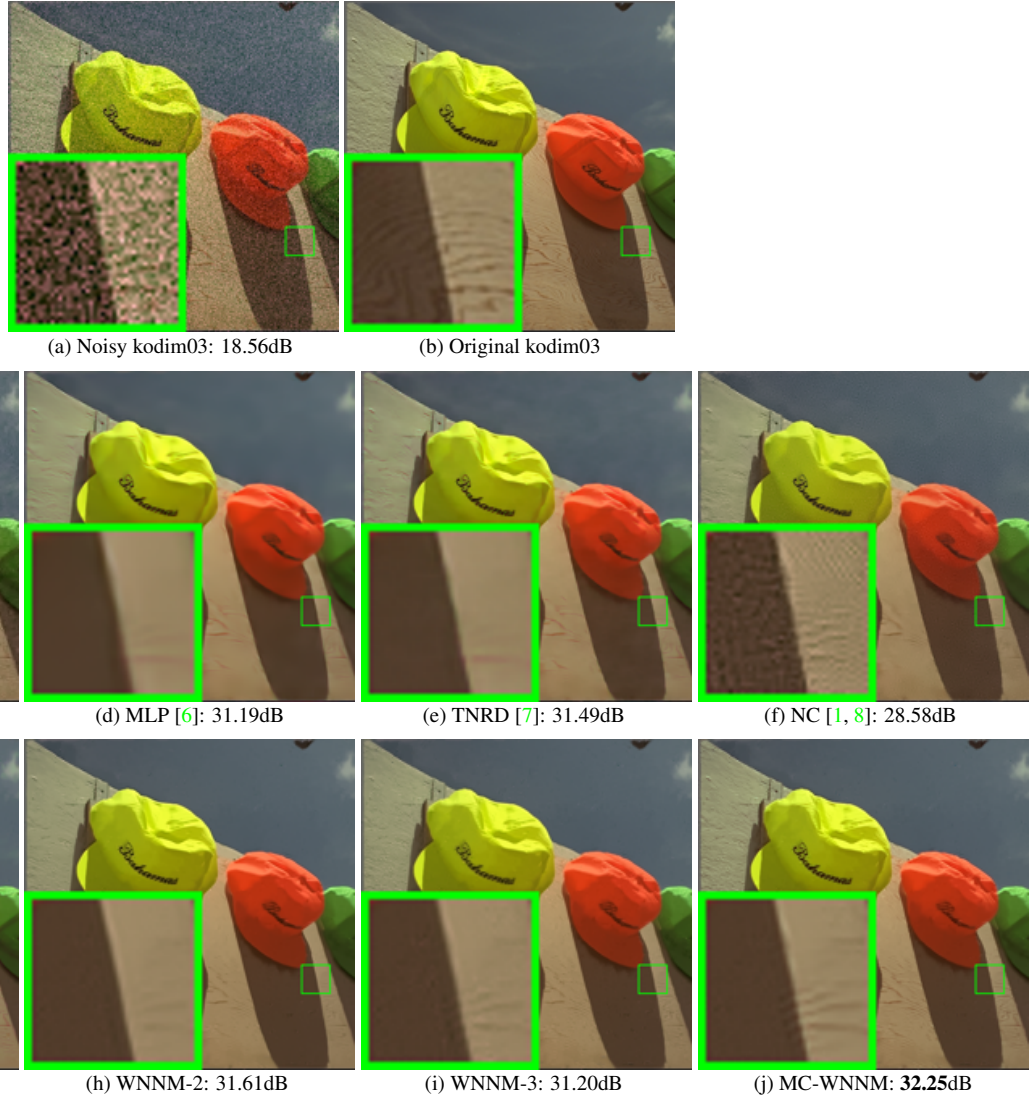
625
626
627
628
629
630
631
632
633
634
635572
573
574
575
576
577
578
579
580
581636
637
638
639
640
641
642
643
644582
583
584
585
586
587
588
589
590
591
592
593645
646
647

Figure 2. Denoised images of different methods on the image “kodim03” degraded by AWGN with different standard deviations of $\sigma_r = 40$, $\sigma_g = 20$, $\sigma_b = 30$ on R, G, B channels, respectively. The images are better to be zoomed in on screen.

648
649
650
651
652
653
654
655
656
657
658
659
660
661
662
663
664
665
666
667702
703
704
705
706
707
708
709
710
711
712
713
714
715
716
717
718
719
720
721
722
723
724
725
726
727
728
729
730
731
732
733
734
735
736
737
738
739
740
741
742
743
744
745
746
747
748
749
750
751
752
753
754
755668
669
670
671
672
673
674
675
676
677
678
679
680
681
682
683
684
685
686
687
688
689
690
691
692
693
694
695
696
697
698
699
700
701

Figure 3. Denoised images of different methods on the image “kodim17” degraded by AWGN with different standard deviations of $\sigma_r = 30$, $\sigma_g = 10$, $\sigma_b = 50$ on R, G, B channels, respectively. The images are better to be zoomed in on screen.

756

757

758

759

760

761

762

763

764

765

766

767

768

769

770

771

772

773

774

775

776

777

778

779

780

781

782

783

784

785

786

787

788

789

790

791

792

793

794

795

796

797

798

799

800

801

802

803

804

805

806

807

808

809

810

811

812

813

814

815

816

817

818

819

820

821

822

823

824

825

826

827

828

829

830

831

832

833

834

835

836

837

838

839

840

841

842

843

844

845

846

847

848

849

850

851

852

853

854

855

856

857

858

859

860

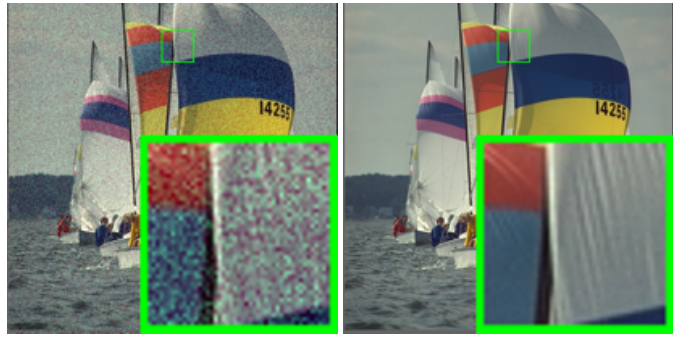
861

862

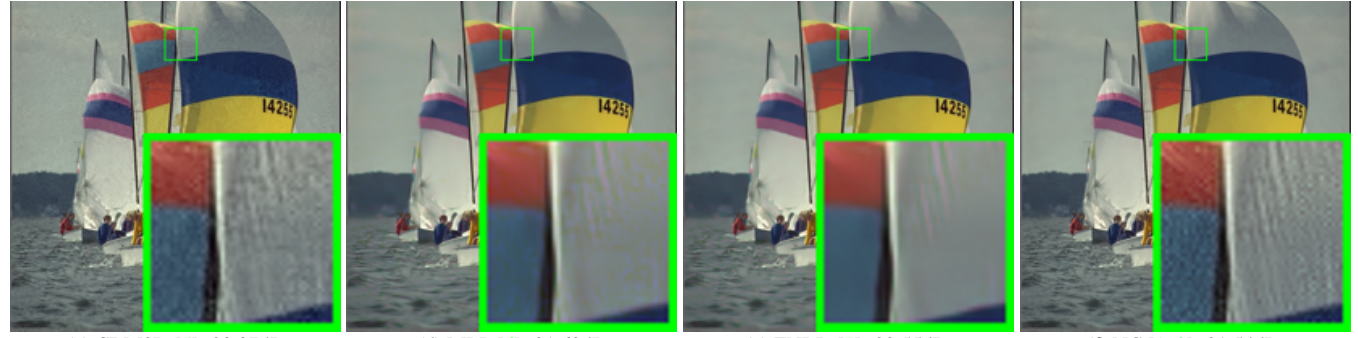
863



Figure 4. Denoised images of different methods on the image “kodim19” degraded by AWGN with different standard deviations of $\sigma_r = 30$, $\sigma_g = 10$, $\sigma_b = 50$ on R, G, B channels, respectively. The images are better to be zoomed in on screen.

864
865
866
867
868
869
870
871
872918
919
920
921
922
923
924
925
926
927
928
929
930
931
932
933
934
935
936
937873
874
875
876
877
878
879
880
881
882
883938
939
940
941
942
943
944
945
946
947
948
949

(a) Noisy kodim09: 22.36dB (b) Original kodim09

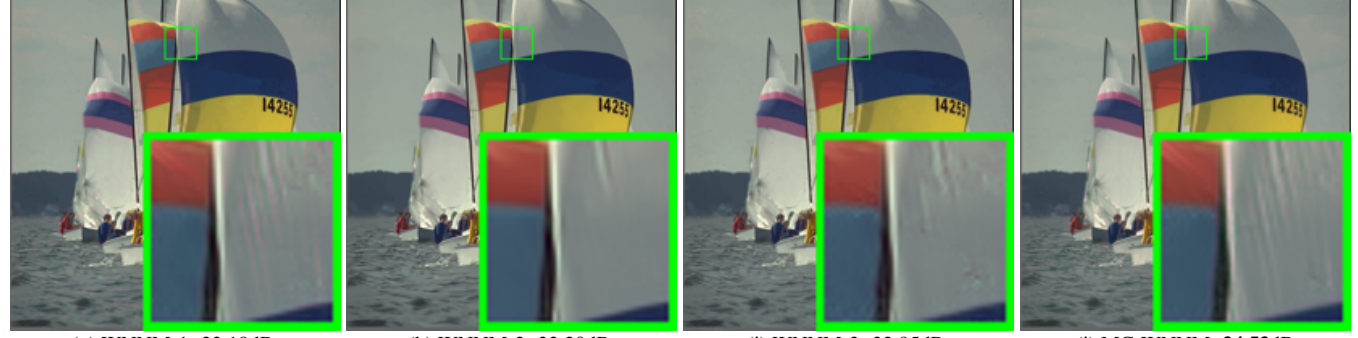


(c) CBM3D [5]: 30.07dB

(d) MLP [6]: 31.63dB

(e) TNRD [7]: 33.55dB

(f) NC [1, 8]: 31.54dB



(g) WNNM-1: 33.19dB

(h) WNNM-2: 33.20dB

(i) WNNM-3: 32.95dB

(j) MC-WNNM: 34.53dB

Figure 5. Denoised images of different methods on the image "kodim09" degraded by AWGN with different standard deviations of $\sigma_r = 5$, $\sigma_g = 30$, $\sigma_b = 15$ on R, G, B channels, respectively. The images are better to be zoomed in on screen.909
910
911
912
913
914
915
916
917950
951
952
953
954
955
956
957
958
959
960
961
962
963
964
965
966
967
968
969
970
971

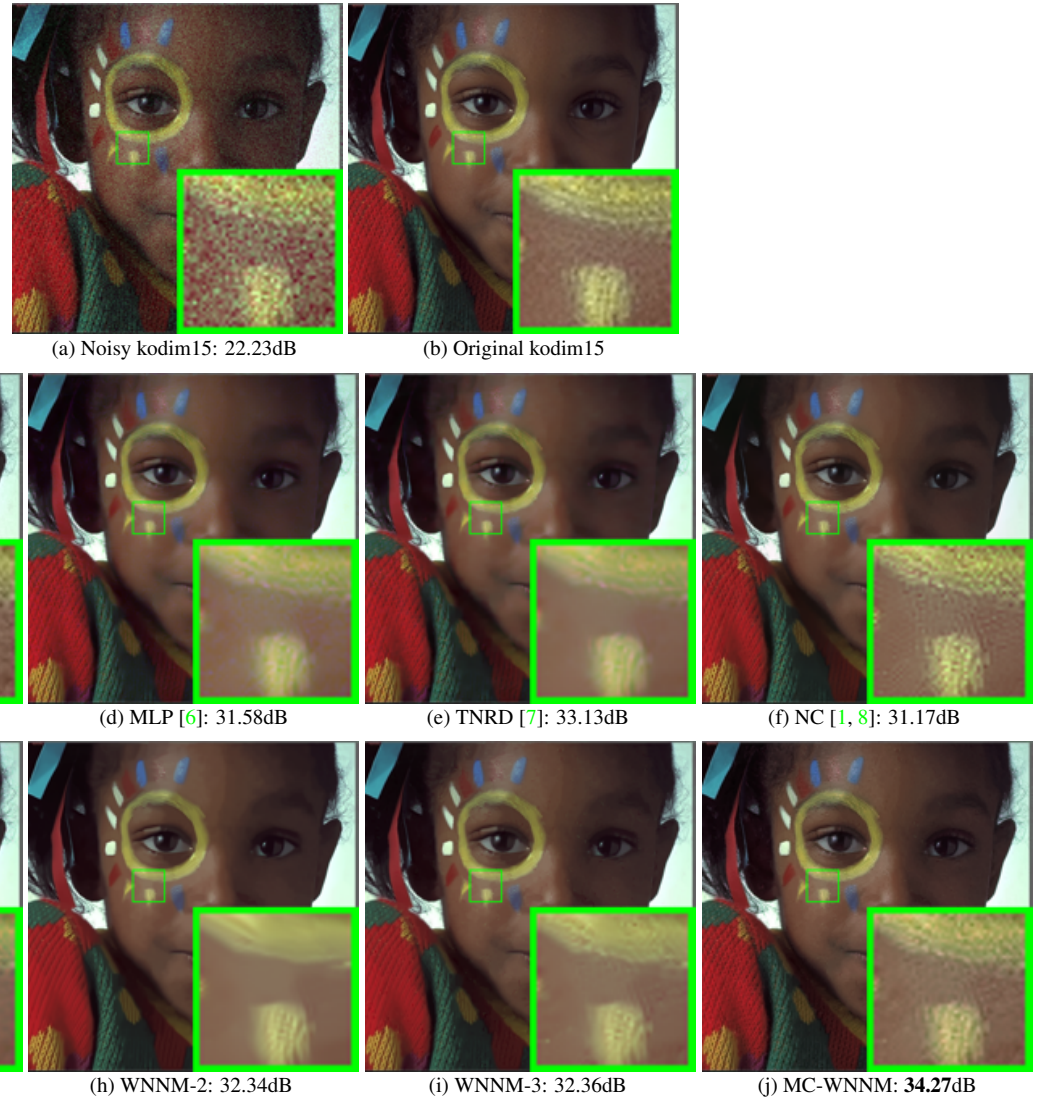


Figure 6. Denoised images of different methods on the image “kodim15” degraded by AWGN with different standard deviations of $\sigma_r = 5$, $\sigma_g = 30$, $\sigma_b = 15$ on R, G, B channels, respectively. The images are better to be zoomed in on screen.

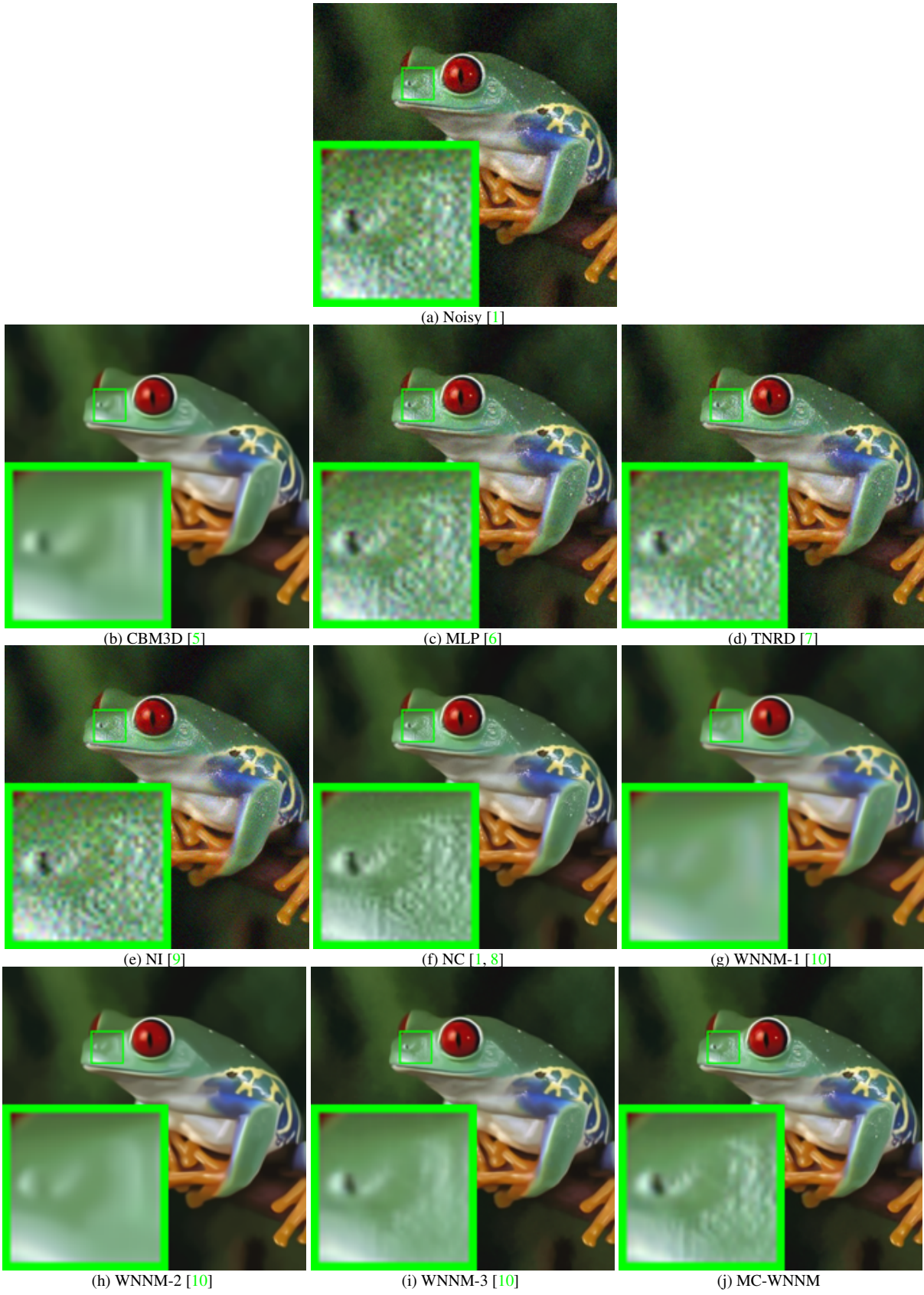


Figure 7. Denoised images of the real noisy image “Frog” [1] by different methods. The images are better to be zoomed in on screen.

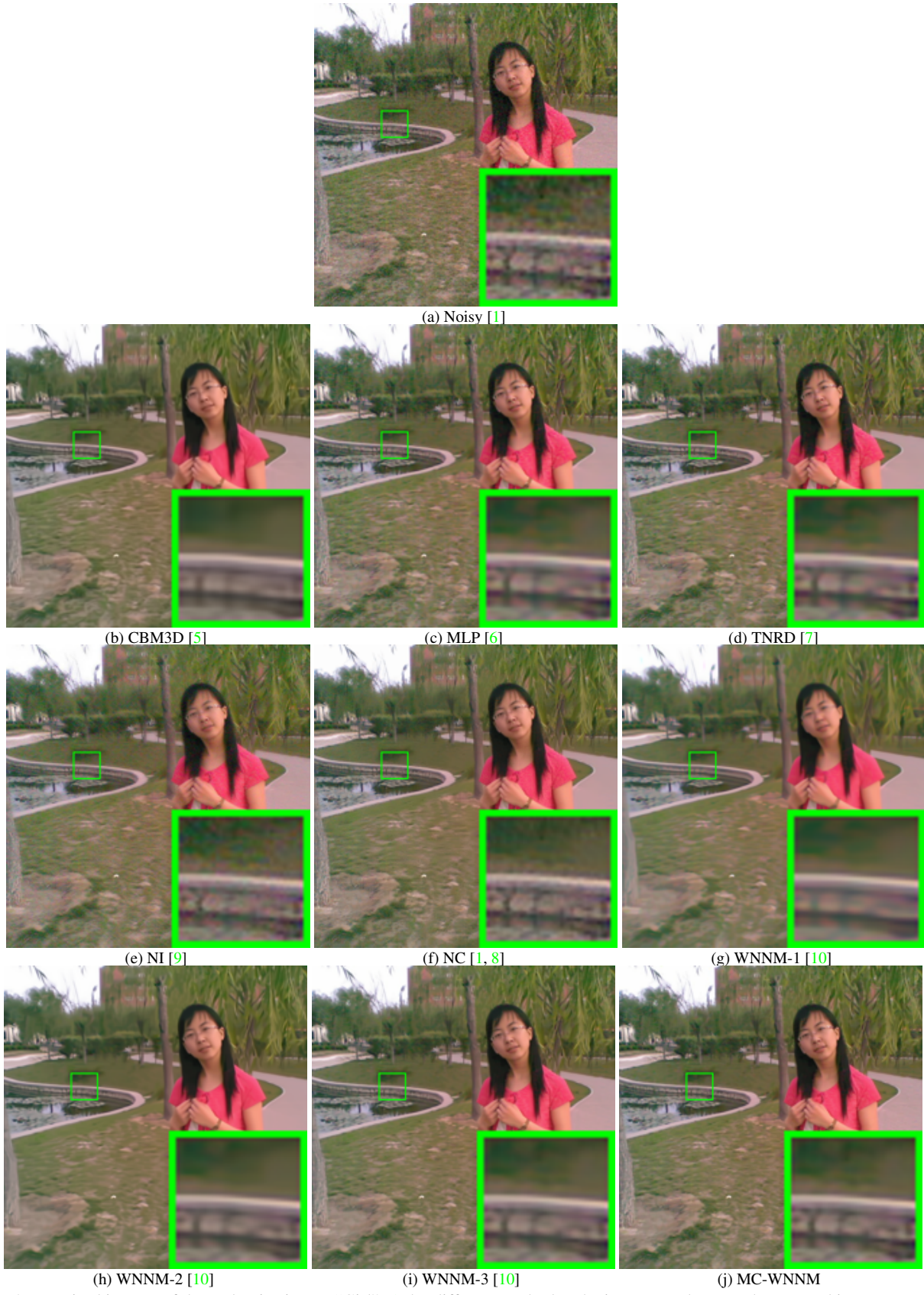
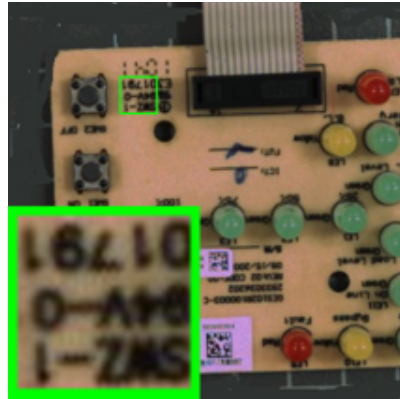


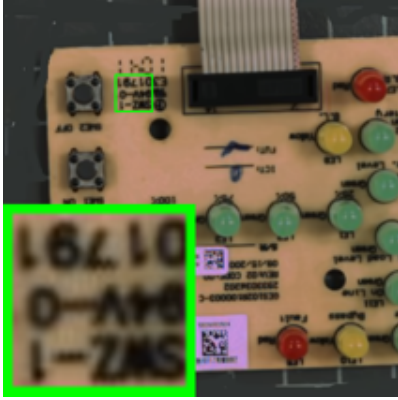
Figure 8. Denoised images of the real noisy image "Girl" [1] by different methods. The images are better to be zoomed in on screen.

1296
1297
1298
1299
1300
1301
1302
1303
1304
1305
1306
1307
1308

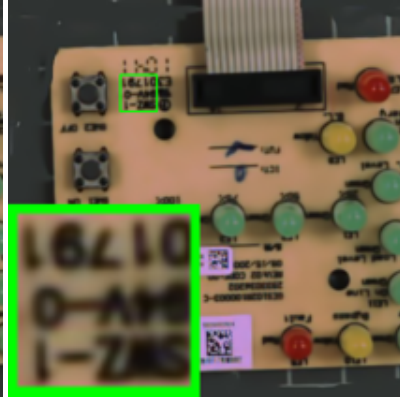
1350
1351
1352
1353
1354
1355
1356
1357
1358
1359
1360
1361
1362



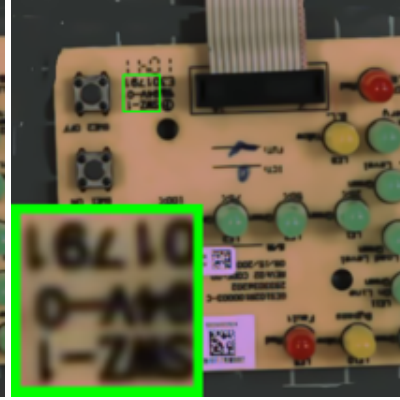
(a) Noisy [1]



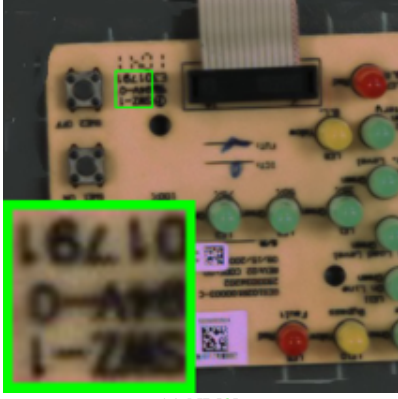
(b) CBM3D [5]



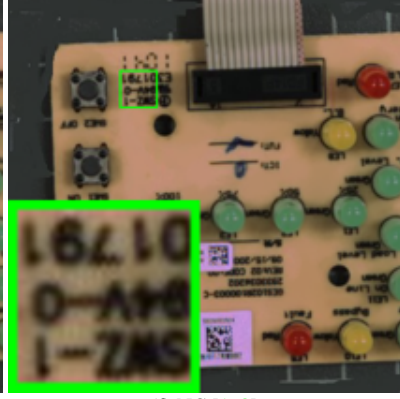
(c) MLP [6]



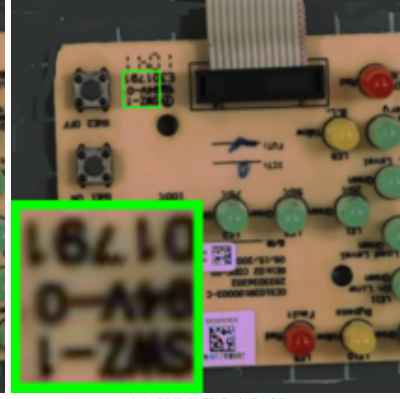
(d) TNRD [7]



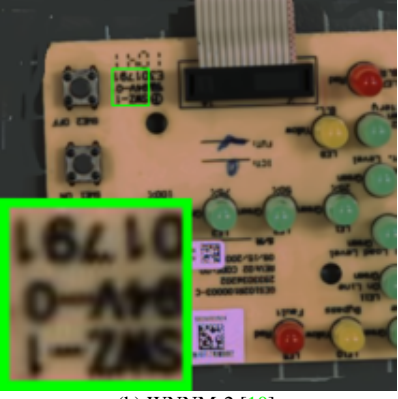
(e) NI [9]



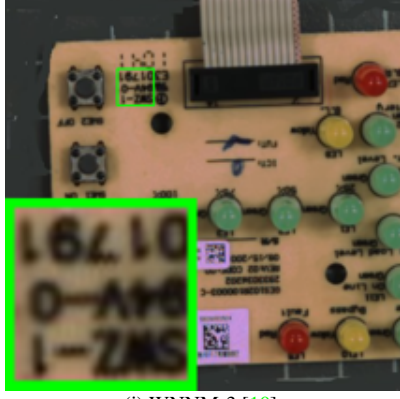
(f) NC [1, 8]



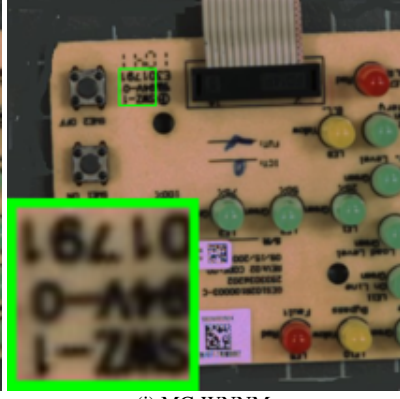
(g) WNNM-1 [10]



(h) WNNM-2 [10]



(i) WNNM-3 [10]



(j) MC-WNNM

Figure 9. Denoised images of the real noisy image “Circuit” [1] by different methods. The images are better to be zoomed in on screen.

1348
1349

1402
1403

1404
1405
1406
1407
1408
1409
1410
1411
1412
1413
1414
1415
1416

(a) Noisy [1]

1417
1418
1419
1420
1421
1422
1423
1424
1425
1426
1427
1428
1429

(b) CBM3D [5]



(c) MLP [6]



(d) TNRD [7]

1430
1431
1432
1433
1434
1435
1436
1437
1438
1439
1440
1441
1442

(e) NI [9]



(f) NC [1, 8]



(g) WNNM-1 [10]

1443
1444
1445
1446
1447
1448
1449
1450
1451
1452
1453
1454
1455
1456

(h) WNNM-2 [10]



(i) WNNM-3 [10]



(j) MC-WNNM

Figure 10. Denoised images of the real noisy image “Room” [1] by different methods. The images are better to be zoomed in on screen.

1458
1459
1460
1461
1462
1463
1464
1465
1466
1467
1468
1469
1470
1471
1472
1473
1474
1475
1476
1477
1478
1479
1480
1481
1482
1483
1484
1485
1486
1487
1488
1489
1490
1491
1492
1493
1494
1495
1496
1497
1498
1499
1500
1501
1502
1503
1504
1505
1506
1507
1508
1509
1510
1511

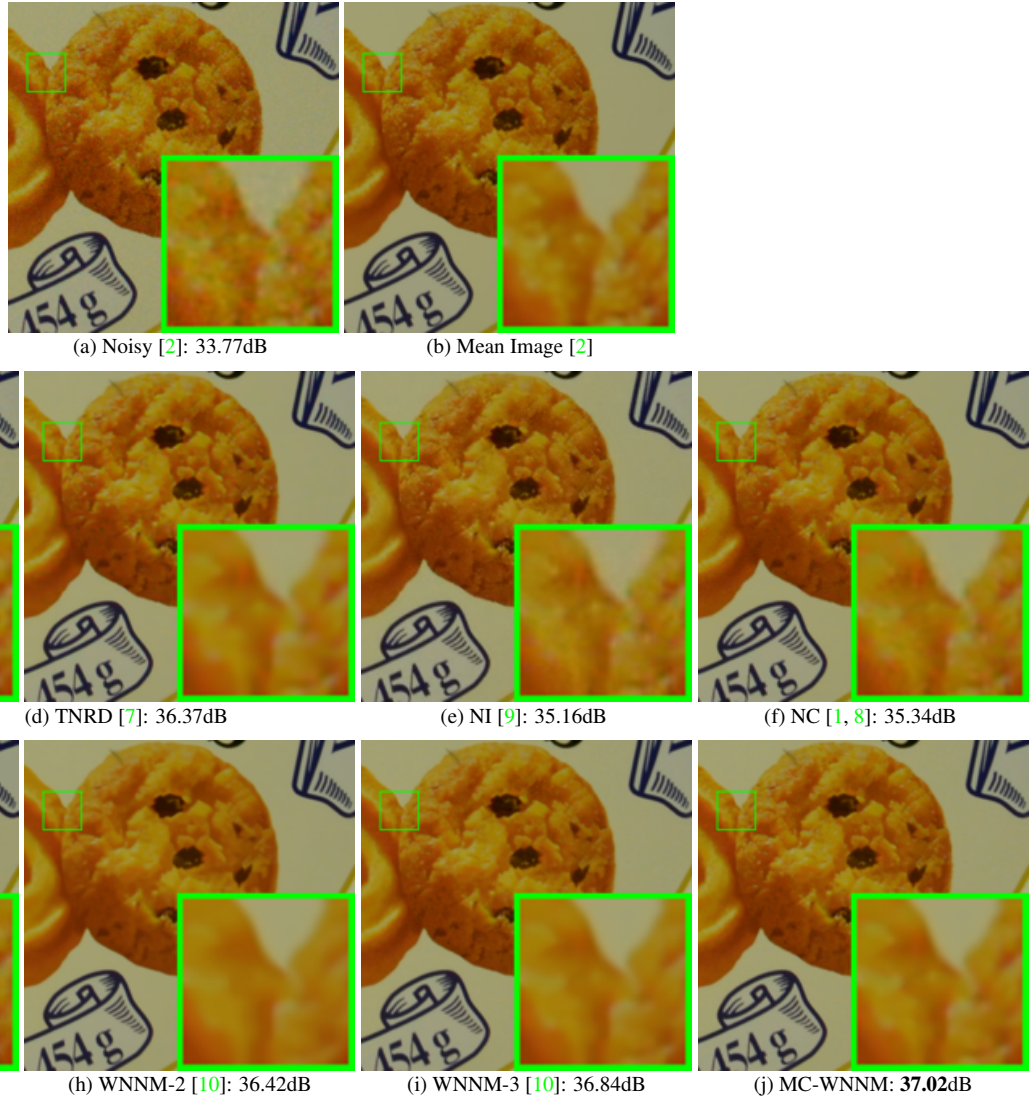


Figure 11. Denoised images of a region cropped from the real noisy image “Nikon D600 ISO 3200 2” [2] by different methods. The images are better to be zoomed in on screen.

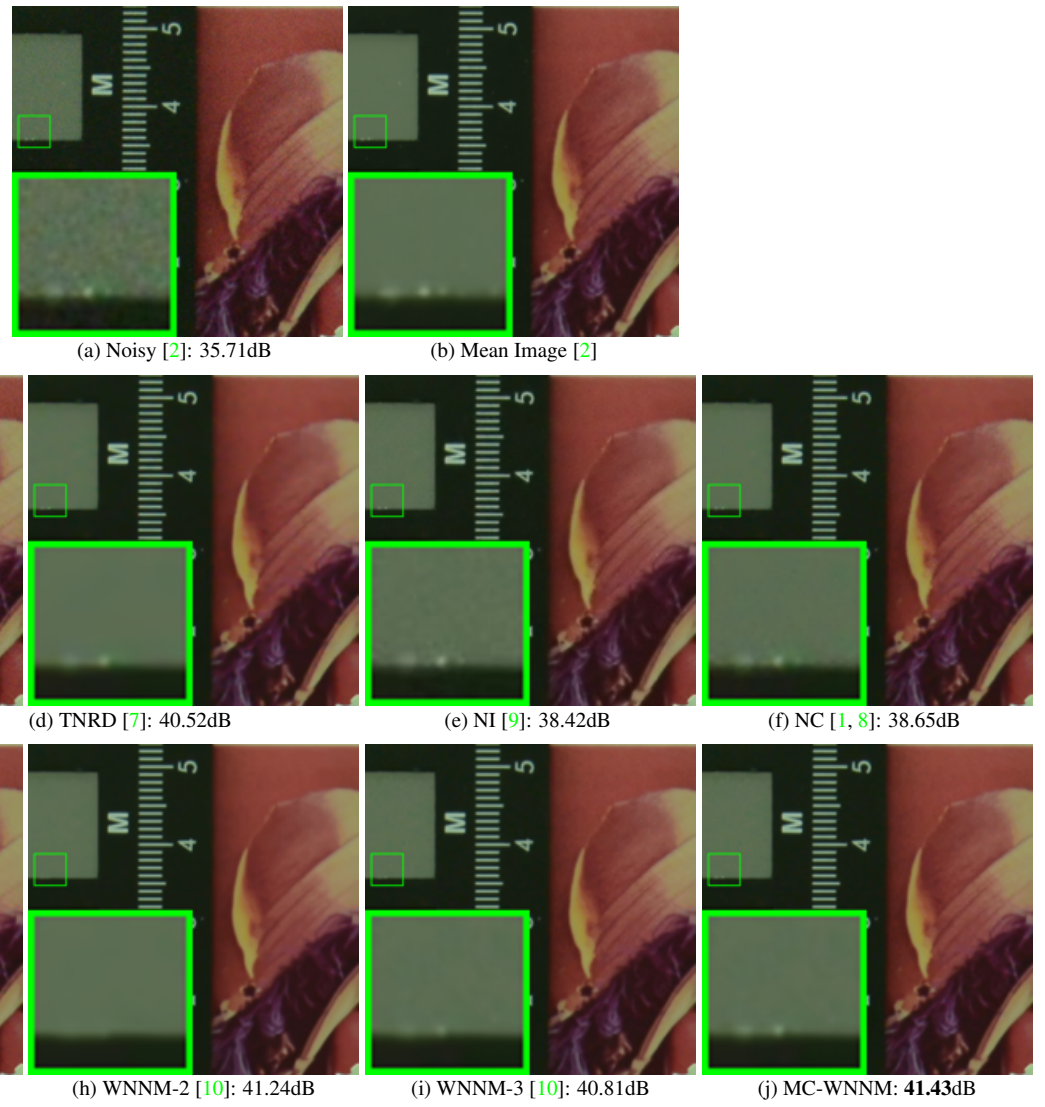


Figure 12. Denoised images of a region cropped from the real noisy image “Nikon D800 ISO 1600 2” [2] by different methods. The images are better to be zoomed in on screen.

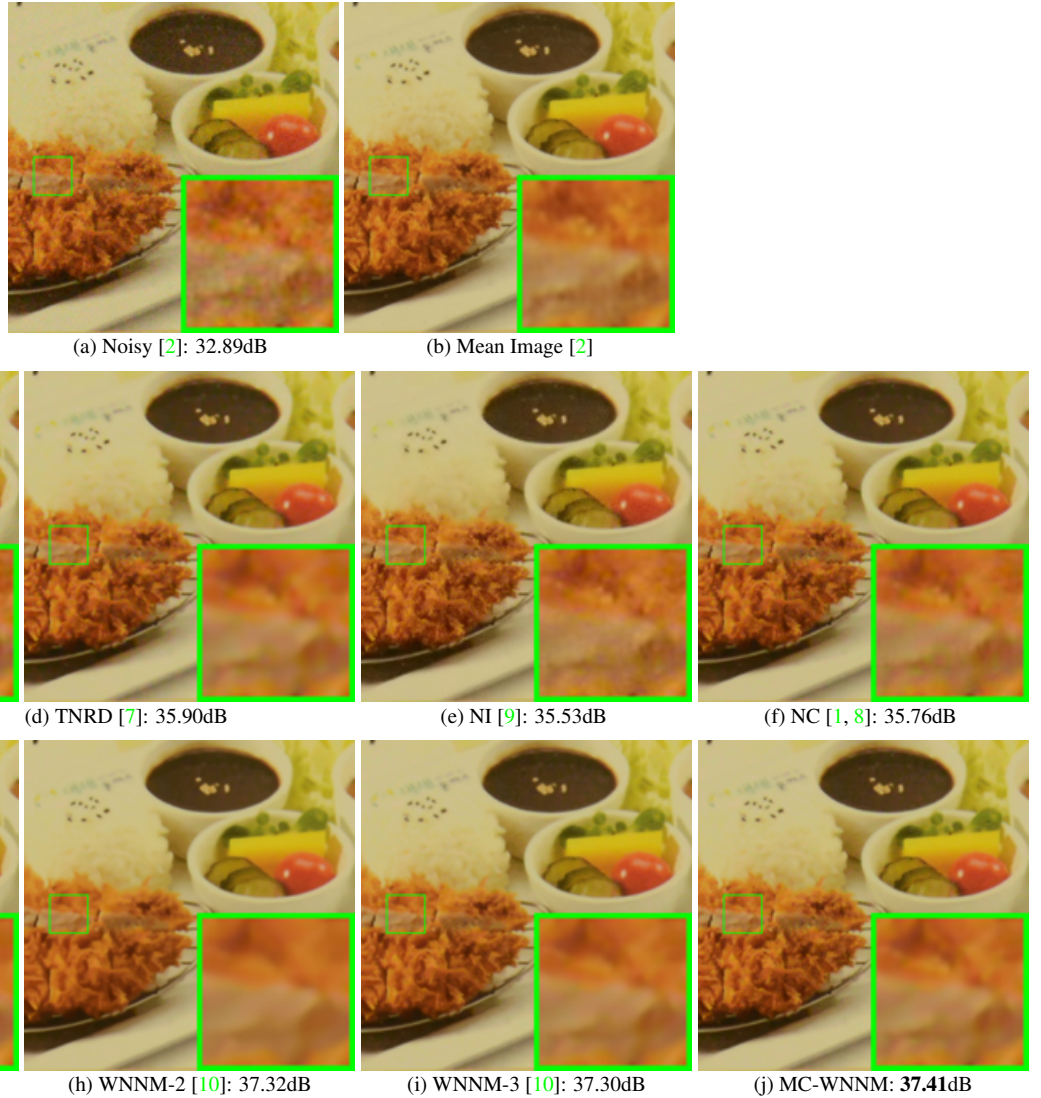


Figure 13. Denoised images of a region cropped from the real noisy image “Nikon D800 ISO 3200 2” [2] by different methods. The images are better to be zoomed in on screen.

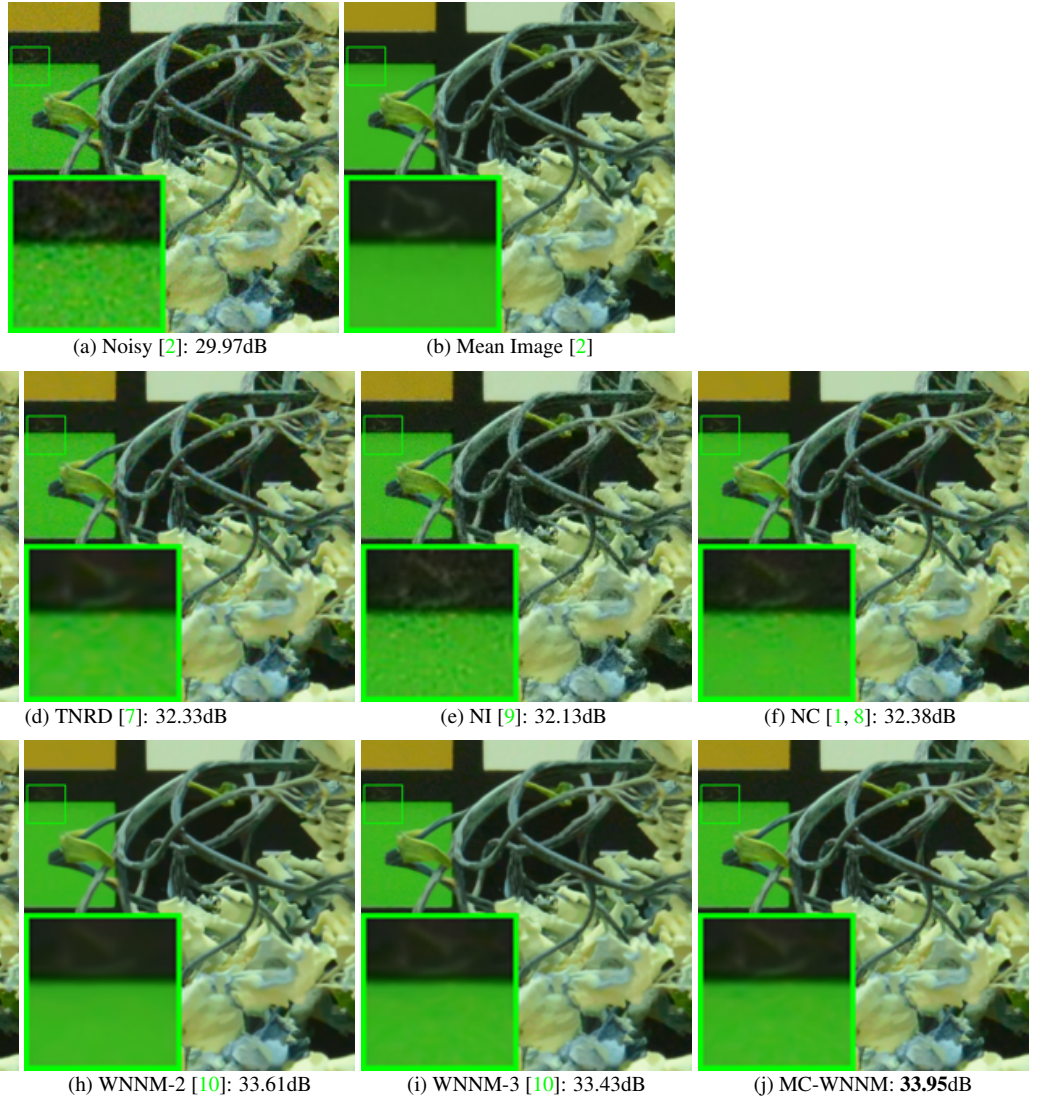


Figure 14. Denoised images of a region cropped from the real noisy image “Nikon D800 ISO 6400 2” [2] by different methods. The images are better to be zoomed in on screen.

1944 **References**

- 1945 1998
1946 [1] M. Lebrun, M. Colom, and J. M. Morel. The noise clinic: a blind image denoising algorithm. [http://www.ipol.im/pub/
1947 art/2015/125/](http://www.ipol.im/pub/art/2015/125/). Accessed 01 28, 2015. 1, 4, 5, 6, 7, 8, 9, 10, 11, 12, 13, 14, 15, 16, 17, 18 1999
1948 2000
1949 [2] S. Nam, Y. Hwang, Y. Matsushita, and S. J. Kim. A holistic approach to cross-channel image noise modeling and its application to 2001
1950 image denoising. *IEEE Conference on Computer Vision and Pattern Recognition (CVPR)*, pages 1683–1691, 2016. 1, 4, 15, 16, 17, 18 2002
1951 2003
1952 [3] C. Eckart and G. Young. The approximation of one matrix by another of lower rank. *Psychometrika*, 1(3):211–218, 1936. 1 2004
1953 2005
1954 [4] S. Gu, Q. Xie, D. Meng, W. Zuo, X. Feng, and L. Zhang. Weighted nuclear norm minimization and its applications to low level 2006
1955 vision. *International Journal of Computer Vision*, pages 1–26, 2016. 1 2007
1956 [5] K. Dabov, A. Foi, V. Katkovnik, and K. Egiazarian. Color image denoising via sparse 3D collaborative filtering with grouping 2008
1957 constraint in luminance-chrominance space. *IEEE International Conference on Image Processing (ICIP)*, pages 313–316, 2007. 5, 2009
1958 6, 7, 8, 9, 10, 11, 12, 13, 14, 15, 16, 17, 18 2010
1959 2011
1960 [6] H. C. Burger, C. J. Schuler, and S. Harmeling. Image denoising: Can plain neural networks compete with BM3D? *IEEE Conference 2012
1961 on Computer Vision and Pattern Recognition (CVPR)*, pages 2392–2399, 2012. 5, 6, 7, 8, 9, 10, 11, 12, 13, 14 2013
1962 2014
1963 [7] Y. Chen, W. Yu, and T. Pock. On learning optimized reaction diffusion processes for effective image restoration. *IEEE Conference 2015
1964 on Computer Vision and Pattern Recognition (CVPR)*, pages 5261–5269, 2015. 5, 6, 7, 8, 9, 10, 11, 12, 13, 14, 15, 16, 17, 18 2016
1965 2017
1966 [8] M. Lebrun, M. Colom, and J.-M. Morel. Multiscale image blind denoising. *IEEE Transactions on Image Processing*, 24(10):3149– 2018
1967 3161, 2015. 5, 6, 7, 8, 9, 10, 11, 12, 13, 14, 15, 16, 17, 18 2019
1968 2020
1969 [9] Neatlab ABSoft. Neat Image. <https://ni.neatvideo.com/home>. 11, 12, 13, 14, 15, 16, 17, 18 2021
1970 2022
1971 [10] S. Gu, L. Zhang, W. Zuo, and X. Feng. Weighted nuclear norm minimization with application to image denoising. *IEEE Conference 2023
1972 on Computer Vision and Pattern Recognition (CVPR)*, pages 2862–2869, 2014. 11, 12, 13, 14, 15, 16, 17, 18 2024
1973 2025
1974 2026
1975 2027
1976 2028
1977 2029
1978 2030
1979 2031
1980 2032
1981 2033
1982 2034
1983 2035
1984 2036
1985 2037
1986 2038
1987 2039
1988 2040
1989 2041
1990 2042
1991 2043
1992 2044
1993 2045
1994 2046
1995 2047
1996 2048
1997 2049
1998 2050
1999 2051